

Influence of secondary gas on control characteristics of ICP-RF plasma torches

P J Bhuyan*^{1,2} & K S Goswami²

¹Department of Physics, Tezpur University
Napaam, Tezpur, Assam. PIN -784028 (India)

²Centre of Plasma Physics- Institute for plasma research,
Nazirakhat, Sonapur, Assam, Pin - 782402(India)

*E-mail: pranjal.bhuyan@rediffmail.com, pjb@tezu.ernet.in

Abstract

Thermal plasma characteristics inside an atmospheric pressure Radio-Frequency (RF) Argon - plasma torch have been studied by numerically solving axis-symmetric 2-D MHD equations, energy transport equations and species conservation equation coupled with 2D Maxwell's equations in the vector potential form. A renormalization group (RNG) $k-\varepsilon$ model was employed to study the turbulence within the torch. Helium is mixed with Argon for injection as the sheath gas, and its effect on the control characteristics of the torch has been studied. A control volume approach and semi-implicit pressure linked equations revised (SIMPLER) algorithm was used to solve the above set of equations to obtain the flow, temperature, turbulence and EM source fields within the torch. Finally, a comparison of the results obtained in our present calculation has been made with other works of similar nature. The torch geometry, flow rates and power dissipation values used in the present calculation are similar to the standard ones available in literature.

1. Introduction

The electrodes in DC plasma [1, 2] are in fact a limitation for their application to high purity material processing because of the contamination of plasma caused by eroded electrode material. In this context, the RF plasma has the advantage of large volume, low velocity, cleanliness and continuity since it is produced by an induction RF electric field without the use of electrodes. RF induction plasma torches are now widely used in different fields, such as processing of high-purity materials, synthesis of ultrafine powders of metals, alloys and ceramics etc [1, 3-11]. An in-depth understanding of the basic plasma processes involved in the operation of RF plasma torches is essential for improving our ability to control them & ensure successful operation of these devices.

Mathematical modeling of the thermal plasma processes gives us an effective and economical tool for studying the torch control parameters, such as flow, temperature and concentration fields inside the induction plasma over a wide range of operating conditions and torch geometry. Moreover, it can be used to probe the areas within the plasma torch where the experimental diagnostics has not been feasible yet. This justifies the amount of research work that has been put into the field of atmospheric pressure [1, 3-11] as well as low pressure [12-13] RF plasma simulation and modeling over the last two decades.

In this paper, we perform a numerical study on the control parameters inside a RF Argon plasma torch operating at atmospheric pressure. We study an inductively coupled RF plasma torch (ICP-RF) with typical geometry [6] and flow conditions with Argon as the working gas. Different concentrations of Helium is mixed with Argon and introduced to the torch as the sheath gas. Diffusion of this gas into the central regions of the torch under different swirling schemes and its effect on the conditions within the torch will be investigated. Turbulence will be studied with a modified $k-\varepsilon$ model, namely the RNG $k-\varepsilon$ model which was earlier applied in the case of RF plasma torch under transient flow conditions [8].

2. Theoretical formulation

2.1. Torch Geometry and basic assumptions

Figure 1 shows the schematic diagram of the RF induction plasma torch and the coordinate system. A summary of torch geometry and operating conditions is tabulated in table 1. The following assumptions are made for the RF induction thermal plasma in order to introduce the governing equations [4]:

- i. The plasma is optically thin continuous fluid in LTE.
- ii. The flow is steady and turbulent with swirling. The velocity, temperature and concentration fields are 2-D and axis symmetric.
- iii. The induction electromagnetic field is 2D and axis symmetric.
- iv. The displacement current, gravity and viscous dissipation, density and temperature fluctuations are not considered.
- v. The effects of anisotropy on the transport properties and on the turbulent structure are not considered.

2.2 Governing equation

Under the given assumptions, the governing equations read in the cylindrical coordinates (z, r, θ) .

The continuity equation:

$$\frac{\partial}{\partial z}(\rho u) + \frac{1}{r} \frac{\partial}{\partial r}(r \rho v) = 0 \quad (1)$$

Momentum equations:

(i) **z- component**

$$\begin{aligned} \frac{\partial}{\partial z}(\rho u u) + \frac{1}{r} \frac{\partial}{\partial r}(r \rho v u) = & -\frac{\partial p}{\partial z} + F_z + 2 \frac{\partial}{\partial z} \left(\mu_{eff} \frac{\partial u}{\partial z} \right) + \frac{1}{r} \frac{\partial}{\partial r} \left[r \mu_{eff} \left(\frac{\partial u}{\partial r} + \frac{\partial v}{\partial z} \right) \right] \\ & - \frac{2}{3} \frac{\partial}{\partial z} \left[\mu_{eff} \left(\frac{\partial u}{\partial z} + \frac{1}{r} \frac{\partial(rv)}{\partial r} \right) \right] \end{aligned} \quad (2)$$

(ii) **r-component**

$$\begin{aligned} \frac{\partial}{\partial z}(\rho u v) + \frac{1}{r} \frac{\partial}{\partial r}(r \rho v v) = & -\frac{\partial p}{\partial r} + F_r + \frac{2}{r} \frac{\partial}{\partial r} \left(r \mu_{eff} \frac{\partial v}{\partial r} \right) + \frac{\partial}{\partial z} \left[\mu_{eff} \left(\frac{\partial u}{\partial r} + \frac{\partial v}{\partial z} \right) \right] \\ & - \mu_{eff} \frac{2v}{r^2} - \frac{2}{3} \frac{\partial}{\partial z} \left[\mu_{eff} \left(\frac{\partial u}{\partial z} + \frac{1}{r} \frac{\partial(rv)}{\partial r} \right) \right] + \rho \frac{w^2}{r} \end{aligned} \quad (3)$$

(iii) **θ - component**

$$\frac{\partial}{\partial z}(\rho u w) + \frac{1}{r} \frac{\partial}{\partial r}(r \rho v w) = \frac{\partial}{\partial z} \left(\mu_{eff} \frac{\partial w}{\partial z} \right) + \frac{1}{r} \frac{\partial}{\partial r} \left[r \mu_{eff} \frac{\partial w}{\partial r} \right] - \rho \frac{vw}{r} - \frac{w}{r^2} \frac{\partial}{\partial r}(r \mu_{eff}) \quad (4)$$

in the above equations, u , v and w are the time-averaged axial, radial and tangential velocity components respectively, p is the pressure, ρ is the density and μ_{eff} is the effective viscosity, which is expressed as the sum of laminar (μ_l) and turbulent (μ_t) parts as

$$\mu_{eff} = \mu_l + \mu_t \quad (5)$$

with

$$\mu_t = \frac{\rho C_\mu k^2}{\varepsilon} \quad (6)$$

Energy equation

The conservation of energy is expressed in terms of enthalpy h as:

$$\frac{\partial}{\partial z}(\rho u h) + \frac{1}{r} \frac{\partial}{\partial r}(r \rho v h) = \frac{\partial}{\partial z} \left[\left(\frac{\kappa}{C_p} + \frac{\mu_t}{\sigma_t} \right) \frac{\partial h}{\partial z} \right] + \frac{1}{r} \frac{\partial}{\partial r} \left[r \left(\frac{\kappa}{C_p} + \frac{\mu_t}{\sigma_t} \right) \frac{\partial h}{\partial r} \right] + Q_j - Q_r \quad (7)$$

Where κ is the thermal conductivity, C_p is the specific heat at constant pressure and σ_t is the Prandtl number, Q_j is the joules heating due to the RF field, and Q_r is the volumetric radiation loss.

The turbulence equations

In the present work, a two-dimensional, time-independent renormalization group (RNG) k - ε model for RF plasma [8] has been used. The time-independent transport equations representing this model are:

$$\frac{\partial}{\partial z}(\rho u k) + \frac{1}{r} \frac{\partial}{\partial r}(r \rho v k) = \frac{\partial}{\partial z} \left[\alpha_k \mu_{eff} \frac{\partial k}{\partial z} \right] + \frac{1}{r} \frac{\partial}{\partial r} \left[r \alpha_k \mu_{eff} \frac{\partial k}{\partial r} \right] + G - \rho \varepsilon \quad (8)$$

$$(9) \quad \frac{\partial}{\partial z}(\rho u \varepsilon) + \frac{1}{r} \frac{\partial}{\partial r}(r \rho v \varepsilon) = \frac{\partial}{\partial z} \left[\alpha_\varepsilon \mu_{eff} \frac{\partial \varepsilon}{\partial z} \right] + \frac{1}{r} \frac{\partial}{\partial r} \left[r \alpha_\varepsilon \mu_{eff} \frac{\partial \varepsilon}{\partial r} \right] + \frac{\varepsilon}{k} (C_1 G - \rho C_2 \varepsilon - R)$$

Here, G represents the production rate of turbulent kinetic energy, given as:

$$G = \mu_t \left\{ 2 \left[\left(\frac{\partial u}{\partial z} \right)^2 + \left(\frac{\partial v}{\partial r} \right)^2 + \left(\frac{v}{r} \right)^2 \right] + \left(\frac{\partial w}{\partial r} - \frac{w}{r} \right)^2 + \left(\frac{\partial w}{\partial z} \right)^2 + \left(\frac{\partial v}{\partial z} + \frac{\partial u}{\partial r} \right)^2 \right\} \quad (10)$$

The RNG $k-\varepsilon$ model is thus similar to standard $k-\varepsilon$ [6,7] model except for the term R , which has the form:

$$R = \frac{C_\mu \rho \eta^3 \left(1 - \frac{\eta}{\eta_o} \right) \varepsilon}{1 + \beta \eta^3} \quad (11)$$

Where $\eta_o = 4.38$, $\beta = 0.012$ and $\eta \equiv S k / \varepsilon$, S being the modulus of mean rate of strain, which is related to G as:

$$S = \sqrt{G / \mu_t} \quad (12)$$

The constants of the turbulence model, as proposed by Launder and Spalding are:

$$C_\mu = 0.09 \quad C_1 = 1.42 \quad C_2 = 1.68 \quad \alpha_k = 1.39 \quad \alpha_\varepsilon = 1.39 \quad \sigma_\varepsilon = 0.7$$

Species conservation equation

In cases where Helium is added with Argon and injected as sheath gas, the concentration of different species is obtained from the species conservation equation:

$$\frac{\partial}{\partial z}(\rho u C_w) + \frac{1}{r} \frac{\partial}{\partial r}(r \rho v C_w) = \frac{\partial}{\partial z} \left[\Gamma_c \frac{\partial C_w}{\partial z} \right] + \frac{1}{r} \frac{\partial}{\partial r} \left[r \Gamma_c \frac{\partial C_w}{\partial r} \right] \quad (13)$$

With $\Gamma_c = \frac{\mu_l}{S_{cl}} + \frac{\mu_t}{S_{ct}}$. For neutral species, neglecting the presence of ions, $S_{cl} = S_{ct} = 1$.

The thermodynamic and transport properties of Ar-He mixed plasma are obtained from the mixture rule [1]. If y_1 and y_2 are the molar fractions and M_1 and M_2 are the molar masses of the two non-polar gases, then

$$\mu = \frac{y_1 \mu_1}{y_1 + y_2 \phi_{12}} + \frac{y_2 \mu_2}{y_2 + y_1 \phi_{21}} \quad (14)$$

With

$$\phi_{12} = \frac{\left[1 + (\mu_1 / \mu_2)^{1/2} (M_2 / M_1)^{1/4} \right]^2}{\left[8(1 + M_2 / M_1) \right]^{1/2}} \quad (15)$$

$$\phi_{21} = \frac{\mu_2}{\mu_1} \frac{M_1}{M_2} \phi_{12} \quad (16)$$

$$y_i = \frac{\frac{C_{wi}}{M_i}}{\frac{C_{w1}}{m_1} + \frac{C_{w2}}{M_2}} \quad (17)$$

$$i = 1, 2$$

The thermal and electrical conductivities are also evaluated from equations similar to equation (14). Finally the specific heat and is deduced from linear interpolation [1]:

$$C_p = y_1 C_{p1} + y_2 C_{p2} \quad (18)$$

The vector potential equations

The electromagnetic field effects produced by the RF field as well as the induced field within the torch is given by the formulation developed by Mostaghimi [3], that gives the real and imaginary components of vector potential as:

$$\frac{1}{r} \frac{\partial}{\partial r} \left(r \frac{\partial A_R}{\partial r} \right) + \frac{\partial^2 A_R}{\partial z^2} - \frac{A_R}{r^2} + \mu_0 \sigma \omega A_I = 0 \quad (19)$$

$$\frac{1}{r} \frac{\partial}{\partial r} \left(r \frac{\partial A_I}{\partial r} \right) + \frac{\partial^2 A_I}{\partial z^2} - \frac{A_I}{r^2} - \mu_0 \sigma \omega A_R = 0 \quad (20)$$

From these equations, we calculate the electric and magnetic fields associated with the flow as:

$$E_\theta = -i\omega A_\theta \quad (21)$$

$$\mu_0 H_z = \frac{1}{r} \frac{\partial}{\partial r} (r A_\theta) \quad (22)$$

$$\mu_\theta H_r = -\frac{\partial}{\partial z} (A_\theta) \quad (23)$$

Finally, the forces and Joules heating terms appearing in the momentum and energy conservation equations are given in terms of the quantities calculated in equations (21)-(23) as:

$$F_z = -\frac{1}{2} \mu_0 \sigma \text{Re}(E_\theta \bar{H}_r) \quad (24)$$

$$F_r = \frac{1}{2} \mu_0 \sigma \text{Re}(E_\theta \bar{H}_z) \quad (25)$$

$$Q_j = \frac{1}{2} \sigma E_\theta \cdot \bar{E}_\theta \quad (26)$$

3. Boundary conditions

At the Entrance ($z = 0$)

$$T_0 = 350 \text{ K}$$

$$u = \begin{cases} \frac{Q_1}{\pi r_1^2} = u_1 & r < r_1 \\ 0 & r_1 \leq r \leq r_2 \\ \frac{Q_2}{\pi (r_3^2 - r_2^2)} & r_2 \leq r \leq r_3 \\ \frac{Q_3}{\pi (R_o^2 - r_3^2)} & r_3 \leq r \leq R_o \end{cases}$$

$$v = 0$$

$$w = \begin{cases} 0 & r < r_2 \\ w_2 & r_2 \leq r \leq r_3 \\ w_3 & r_3 \leq r \leq R_o \end{cases}$$

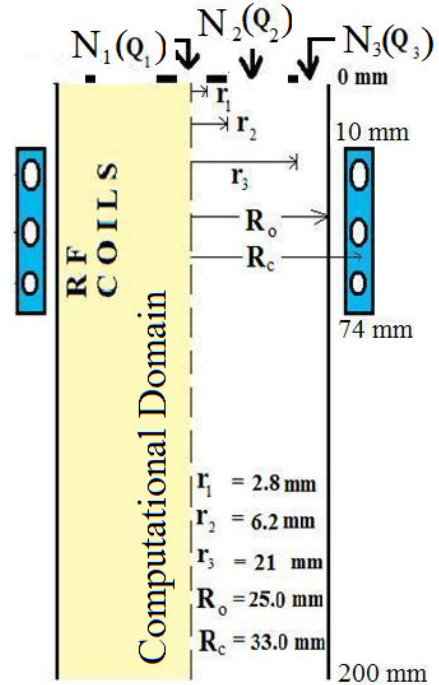


Figure 1- Geometry of the Torch

$$C_w = \begin{cases} 0 & r < r_2 \\ 0 & r_2 \leq r \leq r_3 \\ C_w & r_3 \leq r \leq R_o \end{cases}$$

$$\frac{\partial^2 A_R}{\partial z^2} = \frac{\partial^2 A_I}{\partial z^2} = 0$$

$$k = 0.005 (u^2 + w^2)$$

$$\varepsilon = 0.1 k^2$$

At the exit ($z = 200$ mm)

$$\frac{\partial(\rho u)}{\partial z} = \frac{\partial v}{\partial z} = \frac{\partial w}{\partial z} = 0$$

$$\frac{\partial h}{\partial z} = \frac{\partial k}{\partial z} = \frac{\partial \varepsilon}{\partial z} = \frac{\partial^2 A_R}{\partial z^2} = \frac{\partial^2 A_I}{\partial z^2} = 0$$

At the centerline ($r = 0$)

$$v = w = \frac{\partial u}{\partial r} = 0$$

$$\frac{\partial h}{\partial r} = \frac{\partial k}{\partial r} = \frac{\partial \varepsilon}{\partial r} = A_R = A_I = 0$$

At the wall ($r = R_o$)

$$u = v = w = 0$$

$$k = \varepsilon = 0$$

For the grid points near the wall, the value of turbulent kinetic energy and its dissipation rates, i.e. k_w and ε_w are deduced by the wall functions from the following expression:

$$k_w = \frac{u_\tau^2}{\sqrt{C_\mu}}$$

and

$$\varepsilon_w = \frac{u_\tau^3}{K_a y_p}$$

Where K_a is the von Karman constant ($K_a = 0.41$) and y_p is the first mesh point away from the wall in the computational domain. The frictional velocity u_τ is calculated from:

$$\frac{u_w}{u_\tau} = \frac{1}{K_0} \ln \left(\frac{u_\tau y_p}{\mu} \right) + B$$

Where u_w is the axial velocity at y_p and B is a constant ($B = 5.0$)

Finally, the temperature near the wall is determined from,

$$k_{eff} \frac{\partial T}{\partial r} = \frac{\kappa_c}{\delta_w} (T - T_w)$$

Where δ_w is the tube thickness κ_c is the thermal conductivity of the Plexiglass, and $T_w = 350$ K is the temperature of the outer surface of the tube.

Finally, the boundary condition on Vector potentials is given by:

Table I

Property	Value
Q_1 ($l \text{ min}^{-1}$)	6.3
Q_2 ($l \text{ min}^{-1}$)	30
Q_3 ($l \text{ min}^{-1}$)	150
f (MHz)	3
κ_c ($W \text{ m}^{-1} \text{ K}^{-1}$)	1.047
δ_w (mm)	2
P_o (kW)	8

Table I- Operating parameters of the torch

$$A_R = \frac{\mu_0 I}{2\pi} \left(\frac{r_c}{r_w} \right)^{\frac{1}{2}} \sum_{i=1}^{coil} G(l_i) + \frac{\mu_0 \omega}{2\pi} \sum_{i=1}^{CV} \left(\frac{r_i}{r_w} \right)^{\frac{1}{2}} \sigma_i A_{R,i} S_i G(l_i)$$

$$A_I = -\frac{\mu_0 \omega}{2\pi} \sum_{i=1}^{CV} \left(\frac{r_i}{r_w} \right)^{\frac{1}{2}} \sigma_i A_{R,i} S_i G(l_i)$$

Here, $G(l_i)$ is a function of complete elliptical integrals and CV indicates control volume [3]. The coil current I appearing in the above expression is calculated from the specified total power dissipated into the discharge (P_0). The later can be defined as:

$$P_0 = \int_v Q_j(v') dv'$$

Here Q_j is the local energy dissipation rate, as given in equation 26.

4. Numerical Procedure

A summary of torch geometry and operating conditions is given in figure-1 & table-1. Helium is mixed with Argon & injected through the nozzle N_3 as a sheath gas into the Argon plasma. Swirl is given either at the nozzle N_2 ($= w_2$ m/s) or at the nozzle N_3 ($= w_3$ m/s). In our calculations we have made the inlet swirling proportional to the inlet axial velocity (u_1) of the carrier gas at the nozzle N_1 . We have calculated the control parameters with three values of swirling velocities (w_2 or w_3) amounting to $2u_1$, $4u_1$ and $6u_1$. Numerical calculations are performed both with and without Helium in the sheath gas. For calculations with Helium in the sheath gas, we have considered three inlet concentrations with Helium mass fraction amounting to $C_w = 0.1, 0.3$ and 0.5 .

The governing equations 1-4, 7-9, 13, 19 & 20, along with the boundary conditions are solved using the SIMPLER algorithm developed by Patankar [14]. A non-uniform grid of 55x35 points in the axial and radial directions and a staggered arrangement of variables are used for present calculations. The solution is considered converged when the variation of each field in successive iterations is less than 0.05%. For Benchmarking purpose, in figure 2a,b we have compared our velocity and temperature profiles with the ones obtained in ref [5] under similar conditions. Both the curves show qualitative resemblance. The slight difference in the profile can be attributed to the fact that the work in ref-[5] uses a 1-D electromagnetic formulation, while we are using 2D formulation, where the backflow is expected to be somewhat less.

5. Results and discussion:

5.1. Vector potentials, Joules heating and Lorentz forces

Figure 3a plots a gives the contour plots of A_R (Real part of the vector potential) while figure 3b gives the contour plot of A_I (Imaginary part of vector potential). As seen in the figure, the A_R lies mostly near the tube wall, while A_I

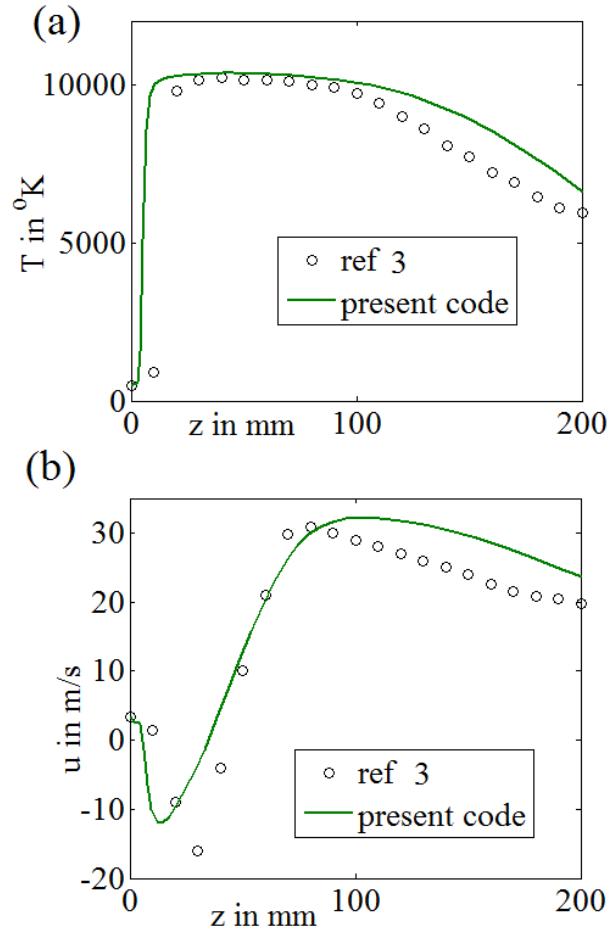


Figure 2: Benchmarking curve comparing our results for (a) centerline temperature and (b) velocity with ref [5] for $Q = 5\text{L/min}$ & $w = 0$. (The turbulence model is same as [5]. However, we have adapted a 2D model for the electromagnetic fields).

moves somewhat inwards, towards the high-temperature regions. The confinement of A_R near the tube wall results from skin effect that prevents the field from penetrating into the hot conducting plasma. A_I is, on the other hand generated by the induced currents within the plasma, and its peak lies on the region where the induced current density is highest. As both the fields are out of phase and as A_I increases with the increase of conductivity of the medium, A_R gets confined to a decreasingly small region of the torch wall. In the typical case shown in figure 3, the maximum of A_I occurs near $r = 15$ mm.

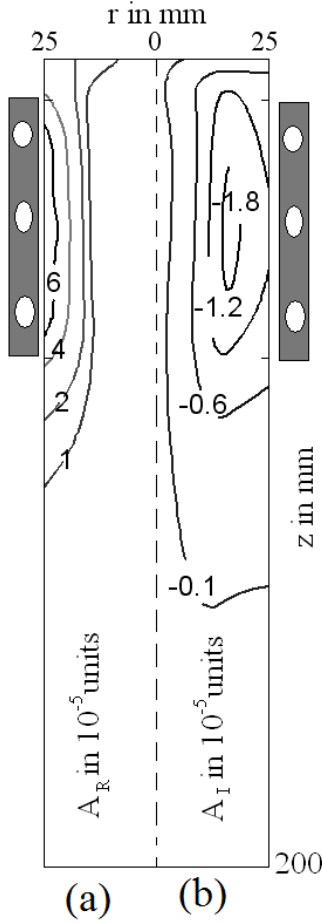


Figure 3: Contour plot of A_R and A_I with swirling $w_2=2u$ and

15 mm, which is also the position where A_I has its peak. The heating of plasma is thus almost entirely due to the induced fields generated through the inductive coupling with the external time-varying current. The radial Lorentz force F_r is all-negative, and hence acts inward, towards the tube axis. F_z is much smaller (generally by a factor of 5-

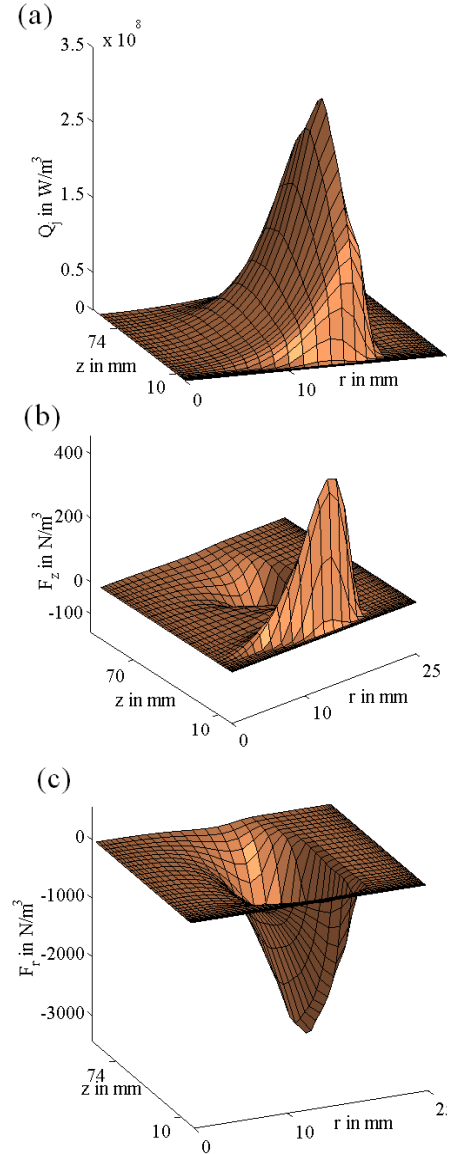


Figure 4: Surface plot of Q_j , F_z and F_r with swirling $w_2=2u$ and $C_w=0.1$.

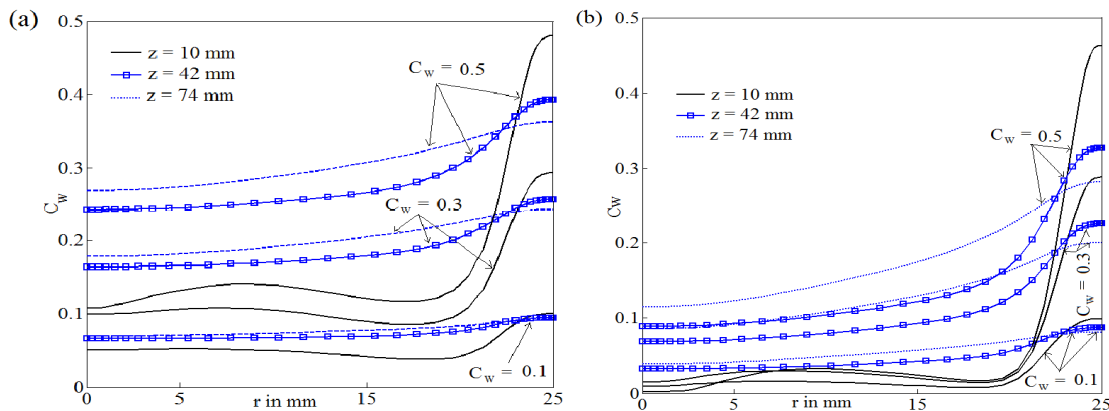


Figure 5: Radial distribution of Helium concentration at the coil entrance ($z = 10$ mm), coil centre ($z = 42$ mm) and coil exit ($z = 74$ mm) for (a) swirling at nozzle N_2 ($w_2 = 4u_1$) & (b) swirling at nozzle N_3 ($w_3 = 4u_1$).

10) as compared to F_r , and has both negative as well as positive components. The effect of F_z is in lowering the backflow caused by electromagnetic pumping on the upstream end of the coil, which is seen as the negative region in the centerline velocity curve (Figure 2b).

5.2. Influence of Swirling on diffusivity of Helium

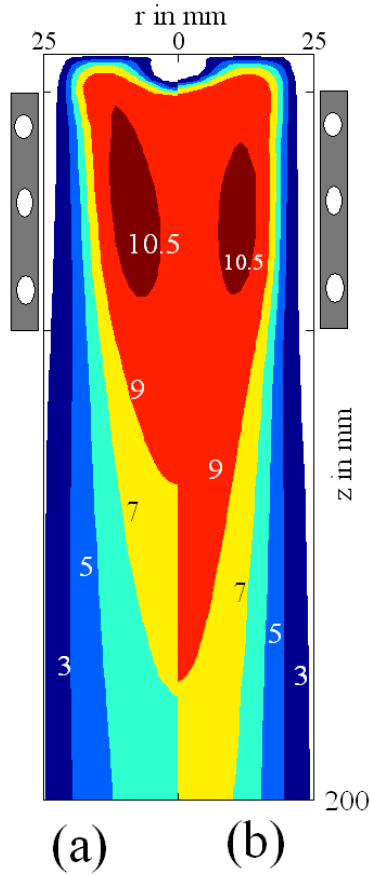


Figure 6: Contour plot of T in $\times 10^3 K$ with $w_2 = 2u_1$ and (a) $C_w = 0.5$ (b) $C_w = 0.1$.

Figure 5a-b plots the distribution of Helium mass fraction at the beginning of the RF coil ($z = 10 \text{ mm}$), at the middle of the coil ($z = 42 \text{ mm}$) and at the end of the coil ($z = 74 \text{ mm}$) for the same amount of swirling ($= 4u_1$) given to the gas injected at Nozzle N_2 and N_3 respectively. Here the curves are plotted for three different Helium mass fraction at the inlet N_3 , namely $C_w = 0.1, 0.3$ & 0.5 . As seen in the graphs, the concentration of helium at the middle and end of the coil region increases almost linearly with the increase in the injection rate of helium in both the cases. However, the concentration of helium at the central region is considerably higher when swirling is applied to the second nozzle (N_2). Helium diffuses considerably from the fringe to the central region by the swirling flow of w_2 .

When swirling is given to gas in the 3rd Nozzle N_3 (figure 5b), the concentration of Helium is found to be much less as compared to the earlier case shown in figure 5a.

This is due to relatively low diffusion caused by swirling flow w_3 . In other words, the mixing process of argon and helium and the diffusion of helium depend strongly on the position of the swirl.

5.3. Influence of Helium on Temperature profile.

Figure 6 plots the contour plot of temperature distribution with swirling $w_2 = 2u$ for two Helium concentrations, $C_w = 0.1$ & 0.5 . Looking at the curves, we see that at the coil region, the high temperature ($T > 10,500K$) region is extended in case of higher injection of Helium (fig 6a). This is because with the diffusion of Helium into the plasma region, the electrical conductivity of plasma decreases. As we have kept the power dissipated to the plasma (i.e. sum of Joule heating over each CV) constant ($P_o = 8kW$), coil current changes to keep the total power constant. Hence the general tendency observed in case of Joule heating is that with increase in the Helium concentration, although the maxima (peak) of the joules heating goes down, its base broadens and the profile diffuses to keep the total power P_o constant.

This increase in T in the central region is not carried to the torch exit and the gas quickly cools down to a much lower temperature due to intermixing of the two gases. In the particular case shown in the figure 6, the maximum exit temperature for figure 6a is found to be about 75% of maximum exit temperature of figure 6b.

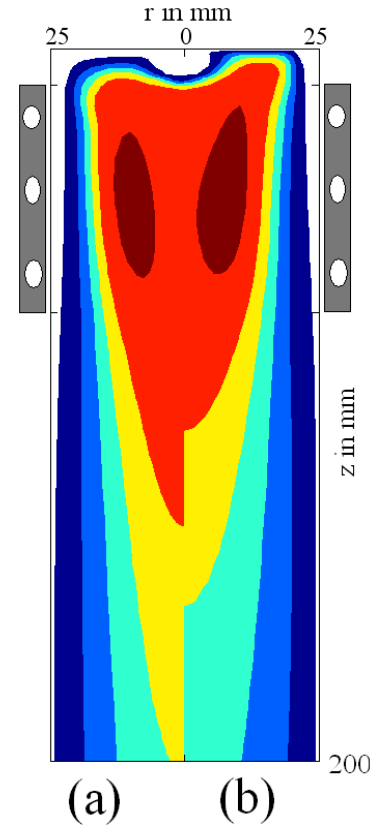


Figure 7: Contour plot of T in $\times 10^3 K$ with $C_w = 0.5$ and (a) $w_3 = 4u_1$ (b) $w_2 = 4u_1$

Coming to the influence of swirling position on the temperature profile, from figure 7a-b, we see that temperature reduces considerably when swirling is given to Nozzle N_2 , as compared to when it is given to the Nozzle N_3 . This is because with swirling given to N_2 , Helium diffuses in a much greater way to the central regions cooling the plasma gas there.

5.4. Turbulence Characteristics

The flow in RF plasma torch is characterized by low velocity and high temperature, and the flow is considered laminar when laminar viscosity is nearly of the same order as turbulent viscosity.

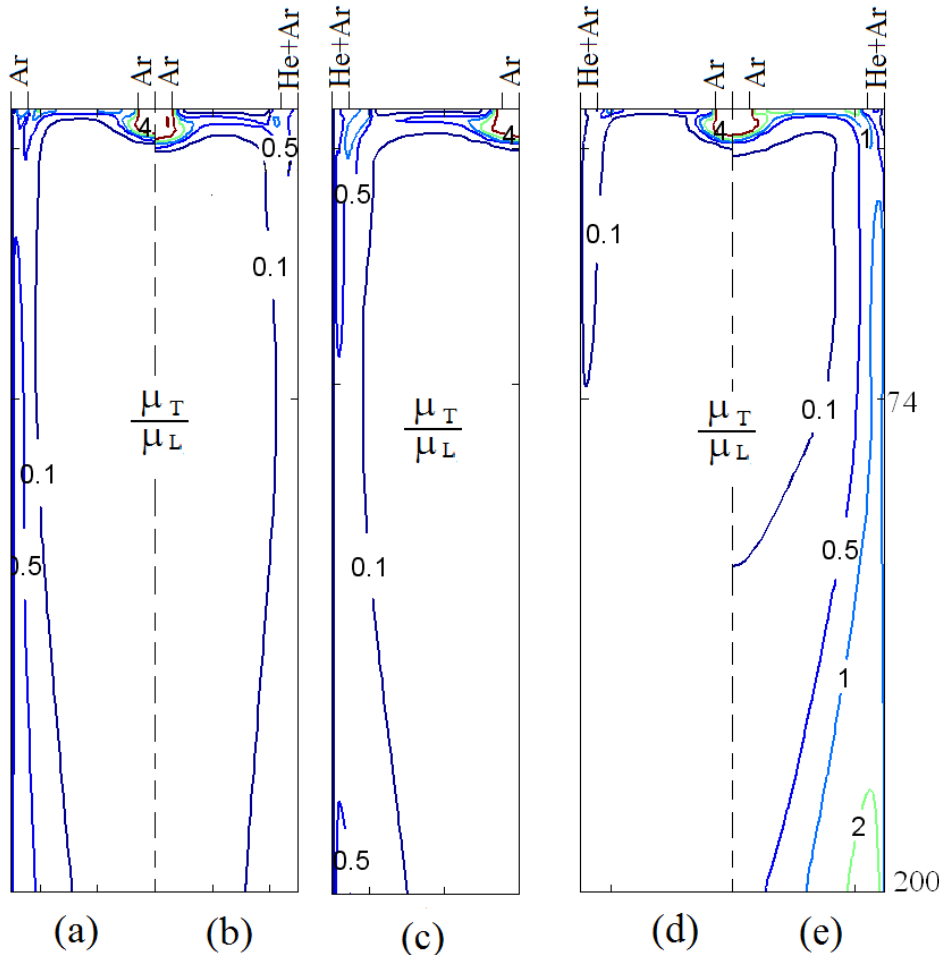


Figure 8: Ratio of Turbulent viscosity to laminar viscosity for (a) $C_w = 0$, $w_3 = 2u_1$ (b) $C_w = 0.5$, $w_3 = 2u_1$ (c) $C_w = 0.5$, $w_3 = 6u_1$ (d) $C_w = 0.5$, $w_2 = 4u_1$ and (e) same as (d), but with standard $k-\epsilon$ model [15] applied instead of the RNG $k-\epsilon$ model.

increase in swirl (figures 8b&c). Also, turbulent viscosity is relatively higher when swirling is given to the nozzle N_3 then when it is given to nozzle N_2 .

Finally, the contours in figure 8d & e plots the laminar to turbulent viscosity ratio as obtained with both RNG $k-\epsilon$ model as well as with the standard $k-\epsilon$ model for the same external conditions. It is found that the turbulence as calculated with the standard $k-\epsilon$ model is much higher as compared to the RNG $k-\epsilon$ model, especially in the hotter regions.

6. Conclusion:

In this paper we have studied the influence of injection of secondary gas (Helium) on the control characteristics of plasma torch. We have studied how the swirling given at different inlet affects the plasma parameters within the torch. Finally we have studied the turbulence within the torch leaning on the RNG $k-\epsilon$ model of turbulence. It is

Figures 8a-e plots the contours for the ratio of turbulent to laminar viscosities

$$\left(\frac{\mu_T}{\mu_L}\right) \text{ for}$$

different flow conditions. It is found that the turbulent regions in our case are mainly confined to the gas inlet and near the wall of the tube. Other regions are found to be predominantly laminar. The turbulence is largest for the case without injection of Helium (figure 8a), while with the increase in injection rate, the amount of turbulent regions goes down. The near wall turbulence increases with

generally observed that when helium is injected into the plasma, the high temperature region reduces. The amount of this reduction depends on how much helium diffuses to the central region. The diffusion is largest, when swirling is given to sheath inlet N_3 .

Turbulence effects decrease with the increase in injection rate of Helium. Also, the turbulence calculated with the present model (RNG $k-\varepsilon$ model) is found to be less compared to the standard $k-\varepsilon$ model.

7. Reference

- [1] Gleizes A, Gonzalez J J and Freton P 2005 *J Phys D: Appl Phys* **38** R153
- [2] Bhuyan P J and Goswami K S 2007 *IEEE Trans on Plas. Sci.* **35** 1781
- [3] Mostaghimi J and Boulos M I, 1989 *Plasma Chem Plasm Proces.* **9** 25
- [4] Nishiyama H, Muro Y, and Kamiyama S 1996 *J Phys D: Appl Phys* **29** 2634
- [5] El-Hage M, Mostaghimi J and Boulos M I 1989 *J Appl. Phys.* **65** 4178
- [6] Merkhoulf A and Boulos M I 1998 *Plasma Sources Sci. Technol.* **7** 599
- [7] Chen K and Boulos M I 1994 *J Phys D: Appl Phys* **27** 946
- [8] Ye R, Ishigaki T and Boulos M I 2004 *J. Appl Phys.* **96** 118
- [9] Mostaghimi J, Dosite M and Jurewicz J 1989 *Canadian J Chem. Engg* , **67**, 929
- [10] P Fauchais 2004 *J. Phys. D: Appl. Phys.* **37** R86
- [11] Heberlein J and Murphy A B, 2008 *J. Phys. D: Appl. Phys.* **41**, 053001
- [12] Tanaka Y 2004 *J Phys D: Appl Phys* **37** 1190
- [13] Morsil E M and Proulx P 2007 *J Phys D: Appl Phys* **40** 4810
- [14] Patankar S V, *Numerical heat transfer and heat flow* 1980 (New York: Hemisphere)
- [15] Launder B E and Spalding D B 1972 *Mathematical Models of Turbulence* (London: Academic)